ENVIRONMENTAL STUDIES

Global expansion of wildland-urban interface intensifies human exposure to wildfire risk in the 21st century

Yongxuan Guo^{1,2}†, Jianghao Wang^{1,2}*†, Yong Ge^{3,4}, Chenghu Zhou^{1,2}

Rapidly increasing human-nature interactions exacerbate the risk of exposure to wildfires for human society. The wildland-urban interface (WUI) represents the nexus of human-nature interactions, where the risk of exposure to natural hazards such as wildfire is most pronounced. However, quantifying long-term global WUI change and the corresponding driving factors at fine resolution remain challenging. Here, we mapped and analyzed the global WUI at 30-meter resolution in 2000, 2010, and 2020. Our analysis revealed that the global WUI expanded by 35.6% since 2000, reaching 1.93 million square kilometer in 2020. Notably, 85% of this growth occurred between 2010 and 2020. The increase in WUI was primarily driven by the unprecedented expansion of global urbanization, contributing an additional 589,914 square kilometer of WUI. In addition, the number of small fires occurring in WUI areas has increased substantially since 2010. These findings underscore the rising wildfire risk to human society and highlight the urgency of implementing tailored fire management strategies in WUI areas.

Copyright © 2024 me
Authors, some rights
reserved; exclusive
licensee American
Association for the
Advancement of
Science. No claim to
original U.S.
Government Works.
Distributed under a
Creative Commons
Attribution
NonCommercial
License 4.0 (CC BY-NC).

INTRODUCTION

The interactions between humans and the natural environment have increased exponentially in the Anthropocene (1). While remote areas may be indirectly affected by teleconnections resulting from human-caused climate change (2, 3), the most immediate conflicts and mutual impacts between human society and Earth system are concentrated in areas where urban border and wildland meet (4–6), an area known as the wildland-urban interface (WUI). The WUI is appealing area for people due to its proximity to nature. This proximity carries a high risk of exposure to natural hazards such as floods, landslides (6), and wildfire (7).

Along with frequent droughts and heatwaves (8), the past two decades have witnessed a substantial increase in the occurrence of extreme and large wildfires (9, 10). These fires have a detrimental impact on human health (11-14), society (15, 16), and the economy (17, 18). Therefore, wildfires demand particular attention among all natural hazards in the WUI. The WUI offers a unique opportunity to observe the complex interactions between humans and wildfires, given the presence of sufficient fuel intermixed with urban areas. People living in or in proximity to WUI areas face an elevated mortality risk due to exposure to flames and the heat of wildfires (13, 19). Wildfire-related smoke can result in an increase in the risk of illness and death in more distant areas, with studies indicating that this risk extends up to 1000 km away (13, 20, 21). Moreover, the fire regime in the WUI is predominantly influenced by human activities. A large proportion of wildfires in the WUI originate from human ignitions (7, 22), such as campfires and cigarette butts, while landscape fragmentation caused by man-made structures limits the extent of wildfires (23). Furthermore, the WUI is the area where the most intensive fire management policies have been implemented (24),

Previous studies have primarily concentrated on mapping the distribution of WUI areas (7, 25-30) or modeling fires in the WUI (31–33), with particular emphasis on fire-prone developed regions, such as the United States (17, 28), Canada, and southern Europe (29). The advent of high-resolution satellite imagery has facilitated the mapping of WUI distributions at finer resolutions (28, 34–36). Recently developed global WUI maps have demonstrated the widespread distribution of WUI areas across continents in 2020 (6, 37). While the rapid growth of WUI areas and the subsequent fire exposure risk have been revealed at local (7) and global scales (37), the existing multiyear WUI maps are relatively coarse at spatial resolution (400 m). A comprehensive investigation of WUI changes at finer resolution is required to assess the effect of wildfires and other potential threats on human communities, such as the spread of zoonotic diseases (38, 39), and to safeguard the biodiversity and ecosystem services in the WUI (39, 40). Furthermore, the direct factors that lead to global WUI changes remain unexplored. Moreover, previous global studies have only examined wildfires within the WUI (6, 37). A quantitative analysis of historical wildfires in and near the WUI could inform the development of more cost-effective mitigation strategies to address this growing threat from wildfires.

Here, we developed global WUI maps at a 30-m resolution using land cover data from multisource satellite images in 2000, 2010, and 2020 to investigate the distribution patterns, temporal changes, and potential wildfire risk represented by WUI areas. First, we derived buffer zones of urban and wildland areas and identified WUI areas globally using the GlobeLand30 dataset. GlobeLand30 contains global land cover products with 10 classes at a 30-m resolution in 2000, 2010, and 2020 (41). The time span of our WUI mapping is 20 years, which allows us to investigate global WUI changes. By detecting land cover changes in WUI areas, we then attributed WUI growth and loss to the land cover change in

¹State Key Laboratory of Resources and Environmental Information System, Institute of Geographic Sciences and Natural Resources Research, Chinese Academy of Sciences, Beijing, China. ²University of Chinese Academy of Sciences, Beijing, China. ³Key Laboratory of Poyang Lake Wetland and Watershed Research, Ministry of Education, Nanchang 330022, China. ⁴School of Geography and Environment, Jiangxi Normal University, Nanchang 330022, China.

^{*}Corresponding author. Email: wangjh@lreis.ac.cn †These authors contributed equally to this work.

and fire-prone regions have witnessed an increasing expenditure on fire suppression (17, 19). Given the frequency of disastrous wildfires in the WUI, it is of great importance to study how and why the WUI has changed globally, with a view to preventing and managing dangerous wildfires.

the urban area and wildland area. Furthermore, we investigated the spatial relationship between wildfires and WUI areas using fire observation data measured by NASA's Moderate Resolution Imaging Spectroradiometer (MODIS). The objective of this study is to examine the distribution and change of the WUI over the past two decades, which could represent potential wildfire exposure risk faced by human society and is crucial for improving fire management policies and mitigating fire-related losses. Our findings will enable fire management departments to develop targeted fire prevention and mitigation strategies and identify the frontiers of wildfire control efforts.

RESULTS

Mapping the global WUI

The WUI indicates where wildfires may pose a direct threat to human society (see Fig. 1A). The criteria for identifying the WUI vary

across regions (see Materials and Methods), here, we defined the WUI as areas where 400-m buffers of wildland areas and 200-m buffers of urban areas overlap. This definition is based on guidelines from the Food and Agriculture Organization (FAO) (42) and further specified in European countries (25). As outlined in the flowchart shown in Fig. 1B, we mapped global 30-m WUI areas in 2000, 2010, and 2020 using urban areas and wildland areas defined by land cover data. Specifically, urban areas, where people commonly gather and interact, are defined by artificial surface. Meanwhile, wildland areas—which include forest, shrubland, and grassland indicate potential fuel sources. We used GlobeLand30 dataset (43) to derive land cover types. Compared to other land cover datasets with coarser resolutions or limited to single year snapshots, the fine resolution (30 m), high accuracy, and long temporal coverage of GlobeLand30 (2000-2020, with a 10-year interval) could provide more information about the WUI distribution and change in both spatial and temporal dimensions.

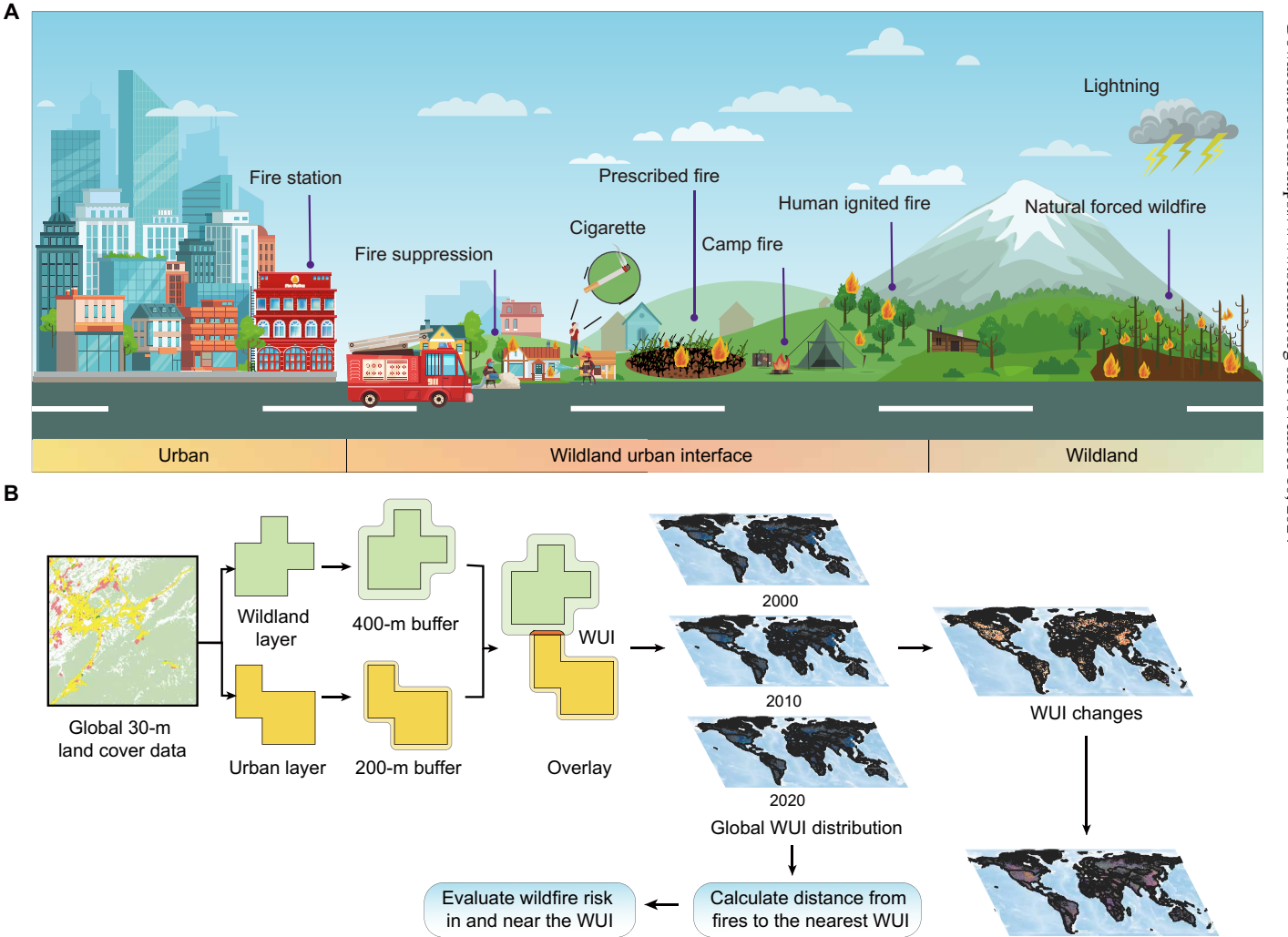


Fig. 1. WUI conception and fire regime over the past two decades. (**A**) Conceptual diagram illustrating how human society and wildfire interact from distant wildlands to densely populated urban areas. (**B**) Workflow we used to map the WUI and identify its changes and direct causes. We generated global WUI maps at 30 m resolution for the yeas 2000, 2010, and 2020 using the GlobeLand30 land cover dataset (*43*). We acknowledge that vector components such as buildings and mountains in (A) are designed by pch.vector/Freepik (www.freepik.com) and vecteezy.com (www.vecteezy.com).

Drivers of WUI changes

We found that global WUI areas have reached 1.93 million km² in 2020, covering 1.44% of the terrestrial area (see Fig. 2). The spatial distribution of the WUI in 2000 and 2010, shown in note S3, followed a similar distribution pattern, scattered across all continents except Antarctica. The Arctic, the deserts of Australia, the Sahara, northern Canada, and Greenland have almost no WUI, mainly due to the low level of human activities. The proportion of WUI areas in a 0.1° grid is relatively low (<20%) in most places (96.89%) in 2020 (Fig. 2B). While only 0.36% of grids have more than 50% of land identified as WUI areas. The majority of WUI areas were located in densely populated regions, such as the southeastern United States, eastern China, and western Europe, which is consistent with published WUI maps in 2020 (see note S4). The three zoomed-in figures of high-density WUI areas in Fig. 2 (D to F) show a typical pattern of the WUI distribution that WUI areas locate radially around urban regions and along roads, suggesting a strong correlation between human activity and potential fire risk to society.

We summarized the regional WUI areas within the 14 regions defined by the Global Fire Emissions Database (GFED) (see fig. S3), which is widely applied to extract regional heterogeneity in global wildfire studies (44–50). The statistics in table S1 reported that the WUI was unevenly distributed across different regions. For example, Temperate North America (TENA), Central Asia (CEAS), and Europe (EURO) contributed the largest WUI in 2020, reaching 478,757 km² (24.80%), 405,607 km² (21.01%), and 199,073 km² (10.31%), respectively. In contrast, there was only a 16,249 km² WUI area in the Northern Hemisphere South America (NHSA), 29 times smaller than in TENA.

We aggregated the WUI map to 0.01° resolution and overlaid it with the WorldPop global population layer (fig. S2). We found that 1.2 billion people lived in the WUI in 2020. Globally, the population density in the WUI (fig. S6) is proportionate to the WUI density shown in Fig. 2B (r = 0.468, 95% CI = [0.466, 0.469], P < 0.001), but there are exceptions. For example, Southern Hemisphere South America had a smaller scale of the WUI than EURO, with more

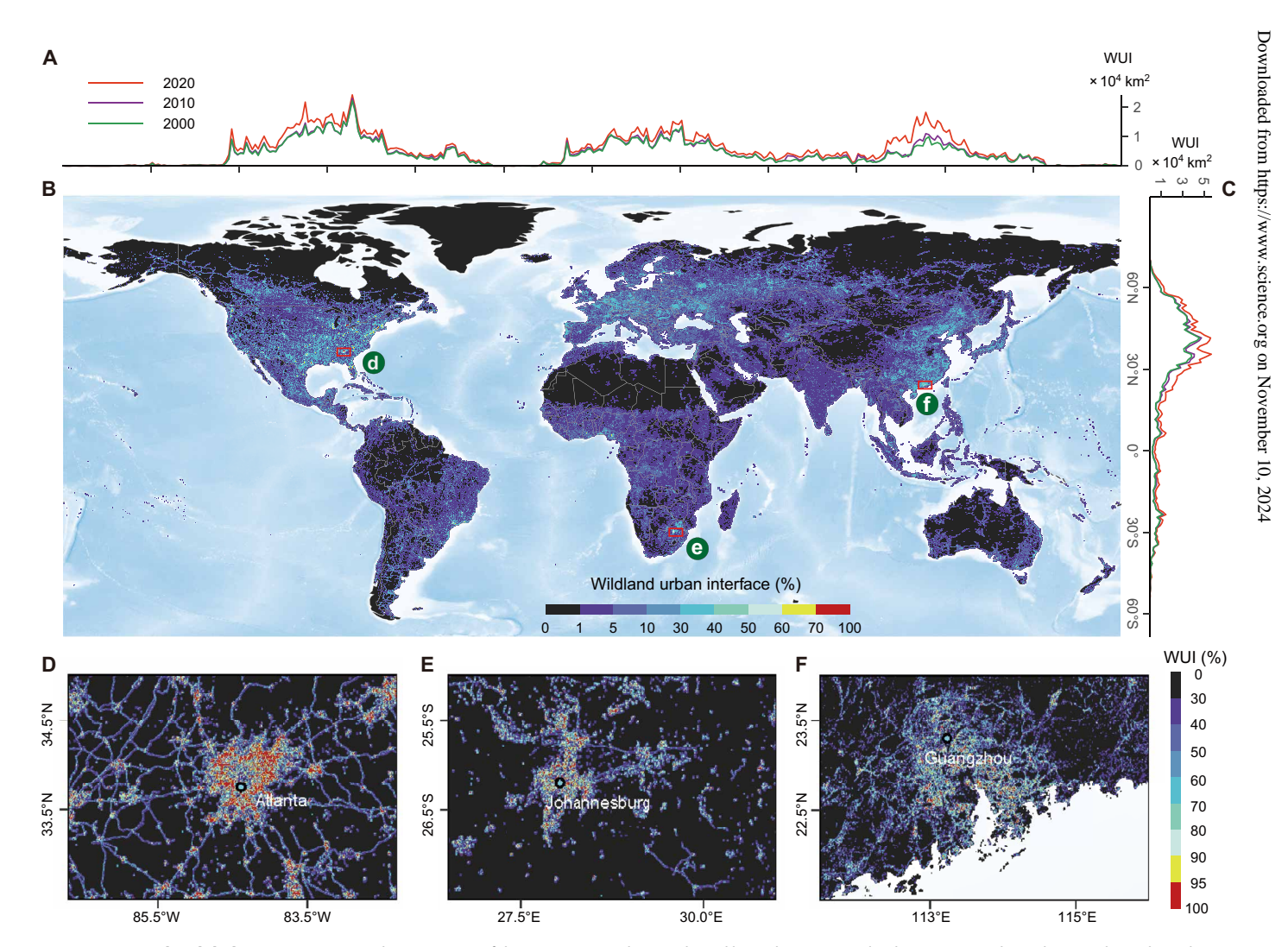


Fig. 2. Mapping the global WUI in 2020. (A and C) Summary of the WUI area at 1° longitude and latitude, respectively. The green, purple, and orange lines show the WUI areas for 2000, 2010, and 2020, respectively. (B) WUI distribution map at 0.1° spatial resolution in 2020. We aggregated the original 30-m WUI map to 0.1° × 0.1° for visualization. The value refers to the WUI proportion (%) of each grid. (D to F) Zoomed-in maps for dense WUI areas (>50%) in Atlanta, United States (D); Johannesburg, South Africa (E); and Guangzhou, China (F), respectively. The maps are shown at a spatial resolution of 0.01°.

people living in the WUI (fig. S7). Note that high population density in the WUI is not necessarily associated with large numbers of people affected by wildfire. Local fire risk can be influenced by many factors in addition to human activities, including fire weather, fuels loads, and fire regimes. For example, the populations in the WUI were relatively small in California and southeastern Australia, while residents in these regions were severely threatened by frequent wildfires over the past decade.

Temporal changes in the global WUI

From 2000 to 2020, the global WUI area according to our WUI maps in 2000, 2010, and 2020 increased by more than a third to a total of 508,161 km². Figure 3A shows a remarkable positive change in the WUI extent clustered in East Asia, mainly due to China's rapid WUI expansion. The Southern Hemisphere, on the other hand,

has remained relatively stable since 2000. Regional decreases in WUI areas were also observed, but increases in WUI areas (>0.5% on a 0.1° grid) were greater than decreases (<-0.5% on a 0.1° grid) (see Fig. 3A and fig. S7). Figure 3A shows that the WUI expansion was most prominently concentrated in the conterminous United States and eastern China since 2000. For example, some regions of Guangdong Province in China and California in the United States have experienced a substantial increase exceeding 30%. In comparison, a shrinking trend of the WUI was evident in various regions, including southeastern Australia, northern Europe, and western Russia. Regions with dense WUI coverage in 2020 are likely to have experienced rapid WUI expansion since 2000. Sub-Saharan Africa, for instance, which has a dense distribution of WUI in 2020, has seen the WUI increased rapidly over the past two decades. However, parts of the northeastern United States and northern Europe, where

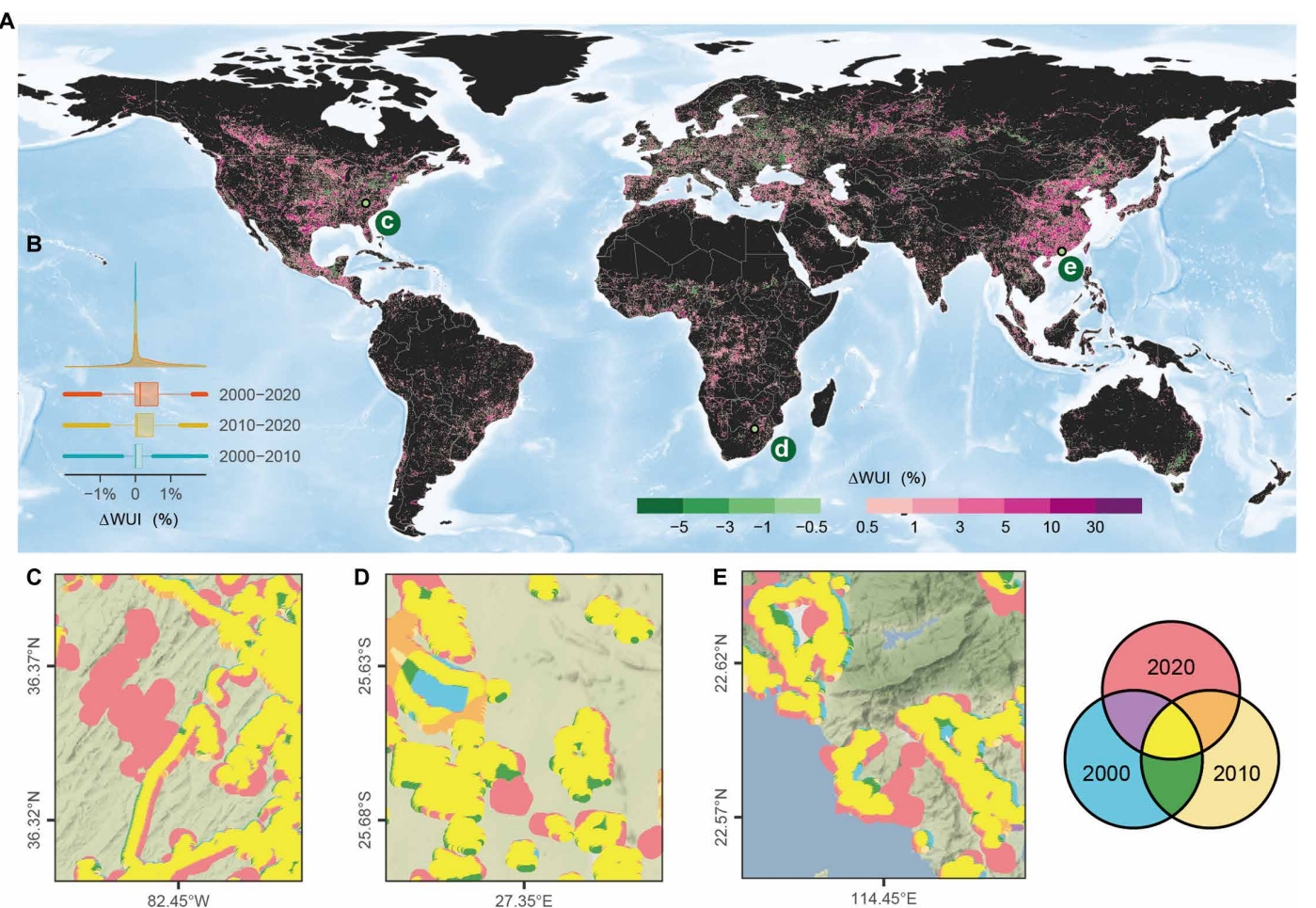


Fig. 3. The spatial extent of the global WUI change during 2000–2020. (A) WUI changes between 2000 and 2020 in a 0.1° grid. The spatial extent of absolute WUI changes is shown in green (areas where the WUI lost) and purple (areas the WUI increased). Grids with slight changes (within $\pm 0.5\%$) are set to transparent. (B) Distributions of WUI changes in a 0.1° grid presented by density plots and box plots. Blue, yellow, and red denote changes in 2000-2010, 2010-2020, and 2000-2020, respectively. The center line and edges of the box represent the median, first quartiles, and the third quartiles, respectively. The whiskers stretch from the box to cover 1.5 times interquartile range. The dense points at both ends of the whiskers are outliers. Given the long-tailed nature of the data, we cut the x axis to display only change within the range of $\pm 2\%$. (C to E) Original 30-m WUI changes in 2000, 2010, and 2020 are shown in three regions located in eastern United States (C), South Africa (D), and Southeast China (E). The colors of pixels correspond to the WUI's existing time, detailed in the right legend. The colors blue, light orange, and pink indicate that the pixel was identified as WUI area in a particular year, 2000, 2010, and 2020. Green, purple, and orange pixels indicate that WUI areas existed in 2000 and 2010, 2000 and 2020, 2010 and 2020, respectively. Moreover, yellow pixels indicate where WUI persisted from 2000 to 2020. The background terrain map was a stamen terrain map provided by the ggmap R package (65).

WUI areas were prevalent in 2020, showed a notable decline in WUI areas from 2000 to 2020. This specific phenomenon could be a result of the decline in the local urban area shown in Fig. 4A.

We further explored the changes of WUI areas in 2000–2010 and 2010–2020 (see fig. S11). We found that most of the new WUI was first identified in 2020, indicating an inconstant rate of global WUI changes during two periods (Fig. 3B). The first decade (2000–2010) contributed only 15% to the total increase in the WUI from 2000 to 2020, while

2010–2020 experienced an astonishing surge, accounting for 85% of the WUI growth. A similar uneven growth rate was also observed in some GFED regions. For example, Equatorial Asia experienced 95.97% of the new WUI between 2010 and 2020, and Boreal Asia even experienced a slight decline between 2000 and 2010 (table S1). Among 14 regions, the lowest contribution of new WUI between 2010 and 2020 was 50.17%, observed in the NHSA. Fig. 3 (C to E) further illustrates the unbalanced growth of WUI areas at 30-m resolution.

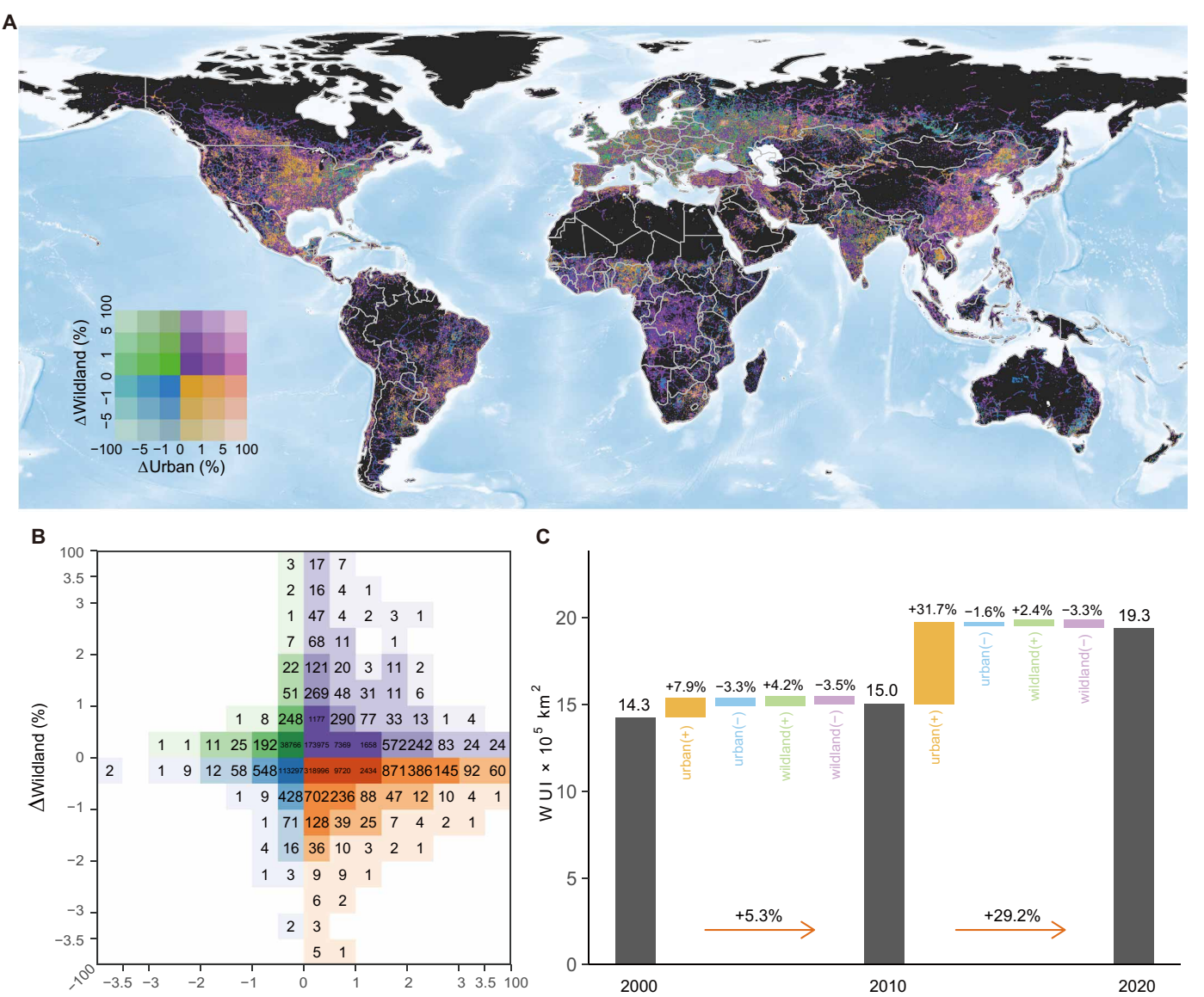


Fig. 4. Land cover change characterizing WUI trends worldwide. (A) Overlapping changes in wildland and urban areas contributed to absolute changes in the WUI (% per 0.1° grid cell) from 2000 to 2020, with colors delineated by the proportion of the WUI shift caused by land cover change. (B) Distribution of grid values from the locations in (A). The heatmap shows grids summed at 1% intervals for both wildland-caused and urban-caused WUI changes simultaneously. The annotation on the heatmap refers to the number of grids in each group. The color classification is consistent with (A). For example, purple represents areas where both urban and wildland changes led to WUI expansion. The color intensity in the heatmap indicates the number of grids summarized by group, with deeper colors representing larger quantities. (C) Global summary of wildland and urban contributions to the WUI change. The black bars show WUI areas in 2000, 2010, and 2020, and the height of the colored bars indicates the WUI change in the corresponding period. Relative changes in 2000–2010 and 2010–2020 were calculated on the basis of WUI areas in 2000 and 2010, respectively.

∆Urban (%)

WUI trends directly impacted by urbanization and wildlands

On the basis of our WUI definition, wildland and urban distribution are the two factors that have directly driven change in the WUI. We found that urban expansion was dominantly responsible for the rapid expansion of the WUI worldwide (Fig. 4, A and C), consistent with an unprecedented growth rate of global urbanization (51). The growth attributed to urbanization of the WUI has reached 589,914 km², which is considerably greater than the net increase in the global WUI from 2000 to 2020. Furthermore, the distribution of 0.1° grid cells supports this conclusion, with most grids experiencing the WUI growth due to urbanization (Fig. 4B). Figure 4C shows a rather weak influence of the remaining factors, including urban area decline and wildland dynamics, on the global WUI change. All factors except urbanization had roughly equivalent contributions to the WUI and remained stationary over the past two decades. However, contrasting phenomena were observed in some regions and countries. For example, vegetation-induced WUI increases overweighted urbanization-related WUI increases in the Middle East (MIDE), EURO, and Southeast Asia (SEAS) according to fig. S13. In addition, the loss of vegetation and urban areas resulted in a large portion of the WUI reduction scattered worldwide

The acceleration of urban expansion resulted in the WUI expanding by 7.9 and 31.7%, respectively, during two periods (Fig. 4C), leading to an abrupt increase in the speed of WUI expansion. At the regional level, a remarkable increase in urban areas changed the spatial pattern of WUI trends in 2010–2020 compared to 2000–2010, such as in eastern Europe and the Democratic Republic of the Congo (fig. S12). Compared to 2000–2010, most GFED regions experienced increased urbanization-related WUI growth in 2010–2020, as reported in table S6. The only exception is EURO, where the growth of WUI areas directly driven by urban areas remained relatively constant.

The patterns between fire activity and WUI

Wildfire risk has increased over the past two decades despite a slight decrease in fire observations (fig. S4, A and B). To investigate the potential for local communities to be exposed to wildfire events in the WUI, we further explored the spatial relationship between WUI areas and wildfire activities. Specifically, to quantify how fire activity and intensity varied with proximity to the WUI, we adopted each MODIS fire observation as one fire hot spot and calculated its distance to the nearest WUI (hereafter Dis2WUI, see Materials and Methods). We selected fire radiative power (FRP) and fire count as critical indexes to represent fire activities in and near the WUI. Fire hot spots were categorized into different FRP ranges (10-MW interval) and by their distance from the nearest WUI (1-km interval). In 2020, there were 1.09% of fire hot spots located in the WUI and 32.29% of fire hot spots located within 5 km of the WUI. Among the 14 GFED regions, CEAS had the most fire hot spots located in the WUI in 2020, with 4.84% of total fire hot spots. Other regions such as TENA, EURO, and MIDE also experienced more than 3% of fire hot spots located in the WUI in 2020 (table S7).

From 2018 to 2022, the majority of fire hot spots, specifically 96.06% in the WUI and 94.23% within 5 km of the WUI, had a FRP of 100 MW or less. As shown in fig. S14B, low-intensity fire hot spots, defined as FRP less than 20.4 MW (50th percentile FRP, calculated from all 2020 fire observations), occurred predominantly within the WUI. In contrast, high-intensity fire hot spots, defined as

FRP greater than 387.6 MW (99th percentile FRP, calculated from all 2020 fire observations), were most likely to occur between 2 and 9 km from the WUI. These zones had more than 1500 fires per year in each 1-km bin (fig. S14C). The large number of wildfires in the WUI supports the hypothesis that the WUI is a fire-prone area where human lives and assets are vulnerable to wildfire and highlights the urgent need to implement more aggressive policies in the WUI when managing fire regimes.

As Dis2WUI increased, the number of fires decreased (fig. S14A). This phenomenon was also evident for all regions except South America (Fig. 5C), where fire intensities appeared to increase slightly with increasing Dis2WUI, suggesting that natural forces (e.g., lightning) may play a greater role in shaping local fire regimes. The stacked top plot in Fig. 5A shows that the relationship between summed FRP and Dis2WUI approximately fits an inverted Ushaped curve for fire hot spots with FRP less than 100 MW and detected within the 5-km buffer of WUI areas. The inflection points of the curves shift away from the WUI as FRP increases, indicating that fire hot spots closer to the WUI tend to burn with less intensity. We also analyzed the change in fire activities. Comparing wildfire records near the WUI from 2008 to 2012 and 2018 to 2022, Fig. 5B shows that fire observations with FRP < 20 MW increased within the 1-km buffer of the WUI. In contrast, fire activities decreased in areas at least 3 km away from the WUI. Similar variation trend was observed in regions such as MIDE and Northern Hemisphere Africa (NHAF). Since 2010, Central America (CEAM), SEAS, and Southern Hemisphere Africa (SHAF) has become more prone to wildfires in and near the WUI (Fig. 5D). The uneven change in human exposure to wildfires since 2010 in and near the WUI may be due to the gradual intensification of human activities and the rapid expansion of the WUI.

DISCUSSION

Understanding wildfire-society interactions requires tracking longterm global WUI changes at fine resolution. However, existing global WUI maps either offer high-resolution (10 m) snapshots for a single year (6) or track changes in the WUI at a coarser resolution (400 m) (37). Using satellite-derived land cover data, our study provided global WUI distribution data with a fine resolution (30 m) available in 2000, 2010, and 2020. By evaluating the temporal change of the global WUI, we revealed the rapid growth of the WUI across the world. A distinctive contribution of our research is to quantify the immediate causes of WUI change that can be directly attributed to the transition from other land cover types to urban and wildland buffers. Previous studies have shown that housing growth is the primary driver of WUI expansion (7, 28) by comparing population growth with housing growth. Using the definition that WUI is where wildland buffers and urban buffers overlap, we first demonstrated that urbanization is a key driver of the WUI expansion, emphasizing the impact of human activities in introducing fire threats to communities. Last, we investigated the pattern of wildfire occurrence not only within the WUI but also in the surrounding regions. We found that low-intensity fire hot spots tend to cluster around WUI areas. Scholars (29, 31) have demonstrated that the frequency of fire ignitions and burn severity are typically lower in densely populated areas by studying building structures in the WUI. Our results therefore confirm these findings on a more macroscale. The fire regimes around the WUI could be a comprehensive result of denser

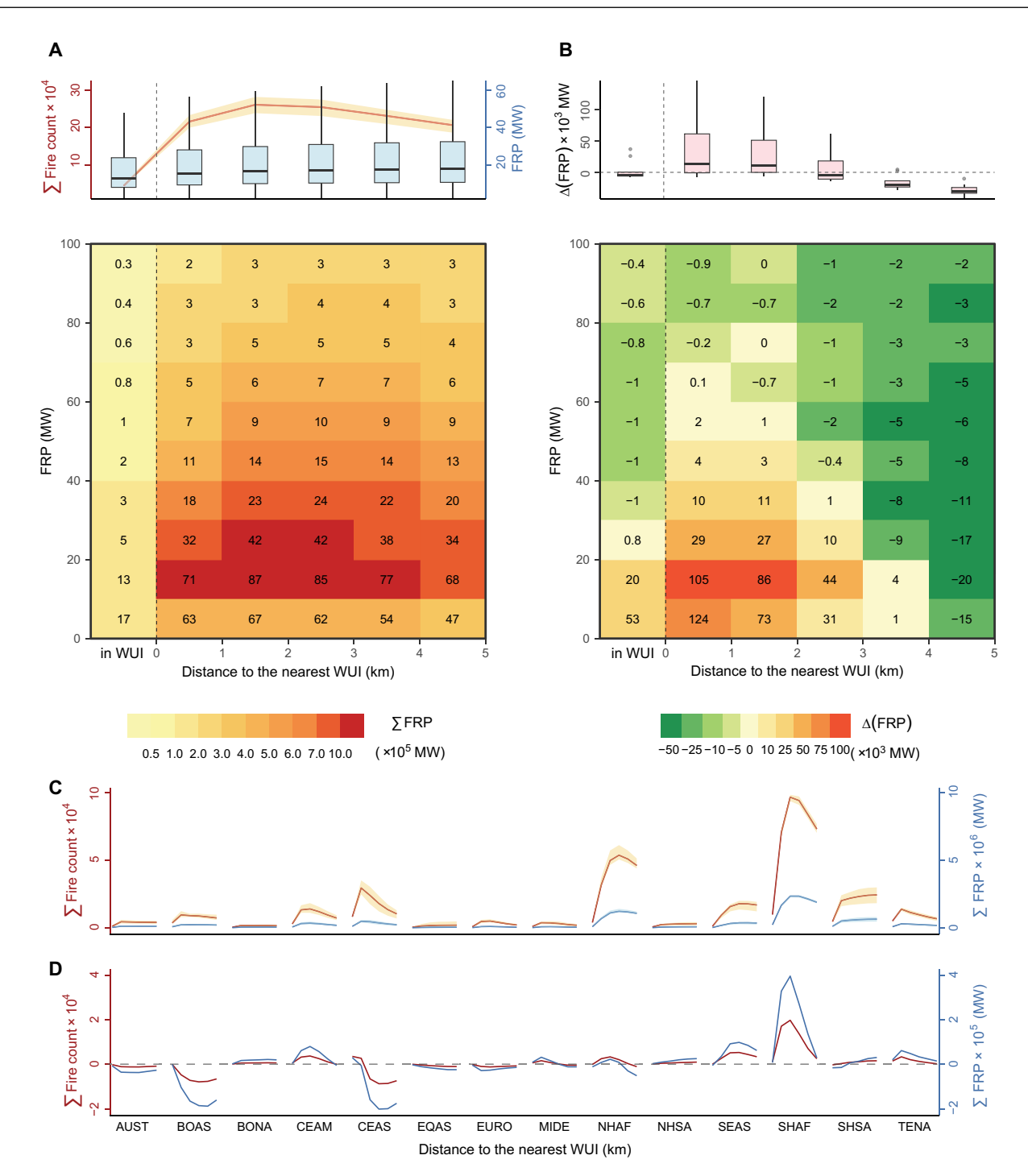


Fig. 5. Spatial characteristics of fires in and near the WUI. (A) Fire activities occurred within a 5 km radius of the WUI from 2018 to 2022, with FRP less than 100 MW, summarized by Dis2WUI and FRP. The yellow line in the top chart represents the mean fire counts in each distance group, while the blue boxplot shows the FRP distribution. (B) Differences in fire activities in and near the WUI from 2008 to 2012 and 2018 to 2022, grouped by Dis2WUI and FRP. The top box plot shows fire FRP distribution within each distance interval. (C) Regional fire activities occurred within a 5-km radius of the WUI from 2018 to 2022 for 14 GFED regions. The red line and the blue line represent mean fire counts and FRP over 5 years, respectively. (D) Regional differences in fire activities in and near the WUI from 2008 to 2012 and 2018 to 2022 for 14 GFED regions. The red and blue lines represent changes in fire counts and FRP, respectively. The x and y axes in the heatmap (A) and (B) denote Dis2WUI and FRP for each fire hot spot. The first column in the heatmap (A) and (B) depicts hot spots falling in the WUI. The numbers on the heatmap are the mean fire counts over 5 years [×10³ in (A) and ×10² in (B)], and the grid color represents the mean value of summed FRP in each group. The shadow areas of lines in (A) and (C) depict the minimum and maximum value of fire counts or FRP from 2018 to 2022. Note that we used the 2010 WUI map to calculate Dis2WUI for fires from 2008 to 2012 and the 2020 WUI map for fires from 2018 to 2022. AUST, Australia and New Zealand; BOAS, Boreal Asia; BONA, Boreal North America; CEAM, Central Asia; EQAS, Equatorial Asia; EURO, Europe; MIDE, Middle East; NHAF, Northern Hemisphere Africa; NHSA, Northern Hemisphere South America; SEAS, Southeast Asia; SHAF, Southern Hemisphere Africa; SHSA, Southern Hemisphere South America; TENA, Temperate North America.

human-caused ignitions, more intensive firefighter resources, and human-caused vegetation fragmentation around the WUI. Our finding reveals that fire occurrences with high FRP value were primarily observed in areas adjacent to the WUI, consistent with previous study that human-ignited fires result in higher fire intensity (52).

Given the different criteria used to identify WUI areas, we reported relatively lower WUI areas and populations living within the WUI. However, our results show a similar spatial pattern to previous WUI maps at both global and regional scales (tables S2 and S4). All three global WUI maps are consistent with regional WUI assessments, for example, showing a high concentration of WUI areas in the eastern United States (7, 53). Steady growth of the WUI has been observed in the conterminous United States from 1990 to 2010 (7) and globally from 1985 to 2020 (37). Our results confirm the upward trend and show that it has steepened since 2010. In Europe, we also found a similar regional WUI spatial pattern that concentrated in western Portugal, Belgium, and the coastline of the Mediterranean (25). However, differences were observed when comparing with WUI patterns mapped at higher resolution, which were based on the definition of the WUI from the U.S. Federal Register. Previous work (28, 53) indicated that the WUI in California was largely concentrated along the western coastline and west of the Sierra Nevada Mountain range, while our evaluation indicated that the WUI was also sparsely distributed in central and southeastern California (fig. S10).

We acknowledge some limitations in our study, particularly regarding the definition of the WUI, the original input data, and uncertainties in data processing. The FAO definition of the WUI considers all built-up areas as urban, ignoring differences in the density of building materials of settlement structures from rural areas to urban centers. By applying a consistent definition of the WUI, we acknowledge that areas where residents are at risk of exposure to wildfires tends to be underestimated in communities proximate to nature while overestimated in a cold or sparsely populated area. Second, because of the limited temporal resolution (10 years) of the input land cover dataset, we could only calculate discontinuous global WUI areas for three versions. Variability in the GlobeLand30 dataset presents another uncertainty, as the availability of input data may have been lower in earlier years. This limitation could be better addressed with more accurate datasets in future. Third, computational errors may occur during data processing, such as merging and resampling raster data. Since uncertainty levels remained constant in 2000, 2010, and 2020, our main conclusion that the WUI is widespread worldwide and has increased markedly over the two decades should remain virtually unchanged. Last, our study only examined the spatial correlation between wildfires and WUI areas, without exploring the interaction between wildfires and human society. Our analysis treated urban areas as synonymous with human society, assuming that the probability of a fire occurring outside the WUI but within urbanized areas was extremely low.

Our 30-m resolution mapping of the WUI could provide a solid foundation for future relevant research. For example, future research could examine a more refined relationship between wildfire and socioeconomic losses using population or other socioeconomic datasets, which could help manage fire regimes more effectively. By using projections of land cover change and climate data under Shared Socioeconomic Pathways, we could further investigate how WUI areas and interior wildfire risk change under different future

scenarios. Because the WUI is not identical to the fire-prone area where wildfires frequently occur and where residents are most likely to be exposed to wildfires, it is critical to identify different levels of fire risk in WUI areas and to identify key factors that influence wildfire risk variability in WUI areas. One possible assumption is that the relationship between human activity intensity and wildfire risk shows an inverted U-shaped pattern. We only examined the direct causes of WUI changes, and more detailed analysis should be conducted in the future to find out the underlying factors that contribute to WUI changes, such as population growth and vegetation cover change.

With this work, we have established a workflow for mapping the WUI that will allow for more convenient updating of the WUI using rapidly developed land cover datasets in the future (54). The global distribution of WUI areas can therefore be a powerful policy tool to address wildfire-related threats at the individual and governmental levels. Governments in countries that have experienced large increase in the WUI since 2000, as shown in our results, such as eastern China, the United States, and Nigeria, should use more policy tools and allocate resources to WUI areas. It is crucial for these regions to strategically control the spread of urban development into wildlands to slow down the growth of WUI areas. More targeted policies and guidelines could be developed areas. More targeted policies and guidelines could be developed and implemented using our fine WUI maps, including reducing fuel loads, educating homeowners, strengthening the patrols, and optimizing fire stations (7). However, because urbanization was the primary driving force behind WUI expansion, it is impossible to effectively address wildfire challenges without preventing vegetation fragmentation. The results of this study demonstrate that governments should fully consider fuel situations when expanding community borders during urban planning. In addition, limited firefighting resources should be allocated to areas within 3 km of the WIII, which have experienced increased wildfires in recent. the WUI, which have experienced increased wildfires in recent years. By leveraging our WUI maps, global insurance companies could also more accurately assess regional fire risks posed to human society and price property insurance policies. At an individual level, residents living in the WUI near vegetation are advised to be cautious about burning open fires in flammable vegetation, as human ignitions tend to exacerbate wildfire hazards around WUI areas (22).

MATERIALS AND METHODS

Experimental design

In this study, we conducted a comprehensive analysis of the global WUI evolution at three time points (separated by 10-year intervals) over a 20-year period from 2000 to 2020, at a high-resolution (30 m) scale. Initially, we created 400-m buffers around wildlands (including forests, shrublands, and grasslands) and 200-m buffers around urban areas using GlobeLand30 (43) land cover data and then delineated the global WUI by overlaying these buffers. The WUI maps in 2000, 2010, and 2020 allow us to investigate how WUI areas change around the world. To further understand WUI dynamic, we analyzed the direct causes of WUI changes at pixel level by comparing the land cover type in different periods. Ultimately, we tried to underline the significance of the WUI in fire management and risk mitigation. With active fires detected by MODIS, we calculated the distance from each fire to the nearest WUI area and illustrated the spatial relationship of wildfires and WUI areas.

Data sources

Global land cover data

Since high spatial resolution satellite images covering the world became available, a bunch of global land cover datasets finer than 100-m resolution have been developed (55, 56). However, most fineresolution land cover datasets only contain a single year release, such as FROM-GLC10 (10-m resolution in 2017), and GLC_FCS30 (57) (30-m resolution in 2015). While GlobeLand30 satisfies high spatial resolution and long temporal coverage, we chose it as the global land cover data to map WUI. Developed with a consistent classification system and methods by the Chinese Ministry of Natural Resources in 2000, 2010, and 2020, GlobeLand30 is a comprehensive set of global 30-m resolution land cover products. The accuracy assessment was conducted using 154,586 samples and more than 230,000 samples for GlobeLand30 V2010 and V2020, respectively, resulting in an overall accuracy of 83.50% for V2010 (with a kappa coefficient of 0.78) and 85.72% for 2020 (with a kappa coefficient of 0.82). The worldwide high spatial resolution, longterm consistency, and reliability made it widely used to monitor land cover change.

GlobeLand30 provides 10 land cover classification types: cultivated land, forest, grassland, shrubland, wetland, water bodies, artificial surfaces, permanent snow and ice, tundra, and bare land. Forest refers to land with trees, with a canopy coverage of more than 30%. Grassland refers to land covered by natural herbaceous vegetation with coverage greater than 10%, including steppe, meadow, savanna, desert steppe, and urban artificial grassland. Shrubland refers to land covered by shrubby with shrub coverage greater than 30%, including montane, deciduous, and evergreen, and desert areas with shrub coverage greater than 10%. Artificial surfaces are formed by artificial construction activities, including all kinds of residential land, industrial and mining facilities, transportation facilities, and more, excluding the contiguous green land and water bodies inside the construction land. The validation of GlobeLand30 V2010 showed that user's accuracy of artificial surfaces, forest, grassland, and shrubland is 86.70, 83.58, 72.16, and 72.64%, respectively. The misclassification within land cover types of wildland (grassland, shrubland, and forest), such as mistakenly labeling shrubland as forest, slightly influenced on the final result. Although the potential urban artificial grassland contained in grassland would lead to exaggeration of WUI areas inside cities. We acknowledge that Globe-Land30 assigned each pixel with a single class, unable to provide information for mixed pixels, which might affect the accuracy of WUI identification.

Active wildfire product

We used MODIS C6.1 MCD14ML active fire product to depict the fire regime nearby the WUI area provided by the Fire Information for Resource Management System (FIRMS). We chose MCD14ML due to its extensive temporal coverage from 2003 to 2020, which facilitates the analysis of spatial relationship between fires and WUI over time. Furthermore, MCD14ML is one of the most widely used fire observation products, containing all Terra and Aqua MODIS fire pixels. The spatial resolution of MCD14ML is 1 km, and the coordinates of each detection are the longitude and latitude of the center point of the 1-km pixel but not exactly where the fire was detected. The overall omission error of fire detections was 86.2%. Generally, the fire size is smaller than the pixel (58). Each record indicates that one or more fires occurred within the pixel, while we

considered each record as an independent wildfire event. The approach implies that larger wildfires extending beyond 1 km² or persisting over several days might be identified as multiple distinct fire events.

The MCD14ML wildfire product provides daily fire information with the latitude and longitude of the fire pixels, observed date, FRP, and more. Four fire types are detected in MCD14ML, including presumed vegetation fire, an active volcano, other static land sources, and offshore fire. We only included fire observations categorized as vegetation fire for analysis. However, we acknowledge that some small fires might not be detected in MCD14ML product out of its relatively coarse spatial resolution, as previous studies revealed (59, 60).

WUI identification and global mapping

The WUI is where wildland and urban areas interact. Because the natural environment and the strength of human activities vary among countries, no worldwide standard identification of WUI areas exists. In North America, most scholars identified the WUI according to the definition published by the U.S. Federal Register (7, 27, 61), which divides WUI into two categories: intermix WUI and interface WUI. Intermix WUI is where man-made structures are densely located with wildland fuel scattered. Interface WUI has a clear boundary between the urban area and the wildland area. In

a clear boundary between the urban area and the wildland area. In Europe, however, the WUI definition maintained a large variety (22). For example, a study in Spain divided the WUI into three groups based on vegetation type (62). In Portugal, the WUI was defined as direct and indirect by reclassifying the land cover map (63).

To enable the production of WUI maps at fine spatial resolution with long temporal series, we used the European identification criterion of the WUI, which was first raised by the FAO (42), based on the definition of WUI areas as where urban buffers and wildland buffers overlay. Under our definition, the WUI is not classified into intermit WIII and interface WIII. The criterion was widely used in intermix WUI and interface WUI. The criterion was widely used in European countries with legal buffer distances ranging from 50 to 200 m for urban areas and 100 to 400 m for wildland areas across different national legal frameworks (25, 64). Considering various fire weather conditions and firefighting abilities across regions, we chose 200 and 400 m as buffer distances for urban and wildland areas. The buffer distances are relatively large to minimize the omission of potentially fire-threatened areas.

As shown in Fig. 1B, we first defined urban layers as artificial surfaces in GlobeLand30. The wildland layer created from the combination of forest, grassland, and shrubland types. We identified the WUI at a 30-m resolution scale. To improve computing efficiency, we first split each 30-m resolution land cover product tile into 400 blocks (around 1500 m in both width and height), each side with a 600-m (20 pixels) buffer to mitigate the edge effect. Subsequently, we separated wildland and urban layers in each block. We generated 200-m buffer zones for urban and 400-m buffer zones for wildland and derived WUI areas by overlapping the wildland and urban buffer zones. To further analyze and summarize the global WUI, we reprojected all 30-m tiles to 0.01° resolution in the WGS84 coordinate system using the average weight method provided by GDAL's gdalwarp function (https://gdal.org/programs/ gdalwarp.html) and merged them into a global map. The pixel value in the 0.01° WUI map refers to the area proportion of WUI areas in each grid. We derived WUI changes in different periods by directly comparing global mosaic WUI maps at 0.01° resolution.

When displaying global WUI distribution and change, we aggregated 0.01° global WUI areas into 0.1° grid cells.

Quantifying the direct causes of WUI changes

The land cover change directly affects WUI changes. Newly increased and lost WUI areas directly caused by the change of urban and wildland. To identify the immediate cause of WUI changes in 30-m pixels, we observed land cover type transformations. For example, if a new WUI pixel newly appeared in 2010 was located in an urban buffer but not located in a wildland buffer in 2000, then the immediate cause of the WUI increase in the pixel is wildland expansion. For pixels where wildland and urban simultaneously lead to WUI change, we assumed that wildland and urban contribute equally, i.e., 50%, respectively. We listed all potential situations of land cover change and the corresponding direct factors of WUI change in table S5. To match the resolution of the global land cover dataset, we identified direct factors of WUI changes at 30-m resolution based on original land cover data used for the WUI identification. Similarly, we transformed direct factors identification results at 30-m resolution into 0.01° global map with two layers, urban contribution and wildland contribution. The values of the aggregated pixel indicate the absolute change of the WUI proportion in the pixel contributed by urban and wildland change. Moreover, the total WUI change proportion in one pixel equals the sum of two immediate causes, i.e., the sum of the urban-related and wildland-related change. We ignored the potential marginal effect when processing merging and resampling of raster data. However, the inaccuracy caused by the marginal effect will not affect the trends in the distribution of WUI areas and its immediate causes, as the data and processing method were kept consistent when generating products in 2000, 2010, and 2020.

Assessing fire regimes nearby the WUI

To better understand how the WUI expansion threatens human society, we analyzed the spatial relationship between wildfire observations and WUI areas. We focused on each detected fire hot spot without combining multiple hot spots into fire events and transformed it into a spatial point with coordinates provided by MCD14ML. Furthermore, the WUI at 30-m resolution was transformed into polygons, merging adjacent WUI pixels. We calculated the great circle distance from points to the border of the nearest WUI polygon. For fire hot spots located in the WUI, the nearest distance to the WUI is set to 0. We assumed that all vegetation fire hot spots were wildfires located either in the WUI or in wildland areas, ignoring a few that were in urban areas. We solely considered fire hot spots with Dis2WUI less than or equal to 5 km, concentrating our study on fire occurrences that are more likely to affect human communities directly. Last, we grouped fire observations by distance to the nearest WUI with 1-km intervals and FRP with 10-MW intervals to display the fire distribution pattern around the WUI.

Supplementary Materials

This PDF file includes:Supplementary Notes S1 to S6
Figs. S1 to S16
Tables S1 to S7
References

REFERENCES AND NOTES

1. S. L. Lewis, M. A. Maslin, Defining the anthropocene. *Nature* **519**, 171–180 (2015).

- E. Weller, S.-K. Min, W. Cai, F. W. Zwiers, Y.-H. Kim, D. Lee, Human-caused Indo-Pacific warm pool expansion. Sci. Adv. 2, e1501719 (2016).
- Y. Yang, L. Wu, Y. Guo, B. Gan, W. Cai, G. Huang, X. Li, T. Geng, Z. Jing, S. Li, X. Liang, S.-P. Xie, Greenhouse warming intensifies north tropical Atlantic climate variability. Sci. Adv. 7, eabg9690 (2021).
- J. R. R. Alavalapati, D. R. Carter, D. H. Newman, Wildland

 –urban interface: Challenges and opportunities. Forest Policy Econ. 7, 705

 –708 (2005).
- J. D. Cohen, Preventing disaster: Home ignitability in the wildland-urban interface. J. For. 98, 15–21 (2000).
- F. Schug, A. Bar-Massada, A. R. Carlson, H. Cox, T. J. Hawbaker, D. Helmers, P. Hostert, D. Kaim, N. K. Kasraee, S. Martinuzzi, M. H. Mockrin, K. A. Pfoch, V. C. Radeloff, The global wildland-urban interface. *Nature* 621, 94–99 (2023).
- V. C. Radeloff, D. P. Helmers, H. A. Kramer, M. H. Mockrin, P. M. Alexandre, A. Bar-Massada, V. Butsic, T. J. Hawbaker, S. Martinuzzi, A. D. Syphard, S. I. Stewart, Rapid growth of the US wildland-urban interface raises wildfire risk. *Proc. Natl. Acad. Sci. U.S.A.* 115, 3314–3319 (2018)
- P. Jain, D. Castellanos-Acuna, S. C. P. Coogan, J. T. Abatzoglou, M. D. Flannigan, Observed increases in extreme fire weather driven by atmospheric humidity and temperature. *Nat. Clim. Change* 12, 63–70 (2022).
- C. X. Cunningham, G. J. Williamson, D. M. J. S. Bowman, Increasing frequency and intensity of the most extreme wildfires on Earth. Nat. Ecol. Evol. 8, 1420–1425 (2024).
- D. M. J. S. Bowman, G. J. Williamson, J. T. Abatzoglou, C. A. Kolden, M. A. Cochrane, A. M. S. Smith, Human exposure and sensitivity to globally extreme wildfire events. *Nat. Ecol. Evol.* 1, 0058 (2017).
- Y. Liang, D. Sengupta, M. J. Campmier, D. M. Lunderberg, J. S. Apte, A. H. Goldstein, Wildfire smoke impacts on indoor air quality assessed using crowdsourced data in California. *Proc. Natl. Acad. Sci. U.S.A.* 118, e2106478118 (2021).
- F. H. Johnston, N. Borchers-Arriagada, G. G. Morgan, B. Jalaludin, A. J. Palmer, G. J. Williamson, D. M. J. S. Bowman, Unprecedented health costs of smoke-related PM_{2.5} from the 2019–20 Australian megafires. *Nat. Sustain.* 4, 42–47 (2020).
- R. Xu, P. Yu, M. J. Abramson, F. H. Johnston, J. M. Samet, M. L. Bell, A. Haines, K. L. Ebi, S. Li, Y. Guo, Wildfires, global climate change, and human health. N. Engl. J. Med. 383, 2173–2181 (2020).
- S. M. Holm, M. D. Miller, J. R. Balmes, Health effects of wildfire smoke in children and public health tools: A narrative review. J. Expo. Sci. Environ. Epidemiol. 31, 1–20 (2021).
- M. A. Moritz, E. Batllori, R. A. Bradstock, A. M. Gill, J. Handmer, P. F. Hessburg, J. Leonard, S. McCaffrey, D. C. Odion, T. Schoennagel, A. D. Syphard, Learning to coexist with wildfire. Nature 515, 58–66 (2014).
- D. B. McWethy, T. Schoennagel, P. E. Higuera, M. Krawchuk, B. J. Harvey, E. C. Metcalf, C. Schultz, C. Miller, A. L. Metcalf, B. Buma, A. Virapongse, J. C. Kulig, R. C. Stedman, Z. Ratajczak, C. R. Nelson, C. Kolden, Rethinking resilience to wildfire. *Nat. Sustain.* 2, 797–804 (2019).
- M. Burke, A. Driscoll, S. Heft-Neal, J. Xue, J. Burney, M. Wara, The changing risk and burden of wildfire in the United States. Proc. Natl. Acad. Sci. U.S.A. 118, e2011048118 (2021).
- D. Wang, D. Guan, S. Zhu, M. M. Kinnon, G. Geng, Q. Zhang, H. Zheng, T. Lei, S. Shao, P. Gong, S. J. Davis, Economic footprint of California wildfires in 2018. *Nat. Sustain.* 4, 252–260 (2021).
- D. M. J. S. Bowman, C. A. Kolden, J. T. Abatzoglou, F. H. Johnston, G. R. van der Werf, M. Flannigan, Vegetation fires in the Anthropocene. *Nat. Rev. Earth Environ.* 1, 500–515 (2020)
- G. Chen, Y. Guo, X. Yue, S. Tong, A. Gasparrini, M. L. Bell, B. Armstrong, J. Schwartz, J. J. K. Jaakkola, A. Zanobetti, E. Lavigne, P. H. Nascimento Saldiva, H. Kan, D. Royé, A. Milojevic, A. Overcenco, A. Urban, A. Schneider, A. Entezari, A. M. Vicedo-Cabrera, A. Zeka, A. Tobias, B. Nunes, B. Alahmad, B. Forsberg, S.-C. Pan, C. Íniguez, C. Ameling, C. De la Cruz Valencia, C. Åström, D. Houthuijs, D. Van Dung, E. Samoli, F. Mayvaneh, F. Sera, G. Carrasco-Escobar, Y. Lei, H. Orru, H. Kim, I.-H. Holobaca, J. Kyselý, J. P. Teixeira, J. Madureira, K. Katsouyanni, M. Hurtado-Díaz, M. Maasikmets, M. S. Ragettli, M. Hashizume, M. Stafoggia, M. Pascal, M. Scortichini, M. d. S. Z. S. Coélho, N. Valdés Ortega, N. R. I. Ryti, N. Scovronick, P. Matus, P. Goodman, R. M. Garland, R. Abrutzky, S. O. Garcia, S. Rao, S. Tratianni, T. N. Dang, V. Colistro, V. Huber, W. Lee, X. Seposo, Y. Honda, Y. L. Guo, T. Ye, W. Yu, M. J. Abramson, J. M. Samet, S. Li, Mortality risk attributable to wildfire-related PM₂₋₅ pollution: A global time series study in 749 locations. Lancet Planet. Health 5, ES79–ES87 (2021).
- T. Xue, G. Geng, J. Li, Y. Han, Q. Guo, F. J. Kelly, M. J. Wooster, H. Wang, B. Jiangtulu, X. Duan, B. Wang, T. Zhu, Associations between exposure to landscape fire smoke and child mortality in low-income and middle-income countries: A matched case-control study. *Lancet Planet. Health* 5, E588–E598 (2021).
- J. K. Balch, B. A. Bradley, J. T. Abatzoglou, R. C. Nagy, E. J. Fusco, A. L. Mahood, Humanstarted wildfires expand the fire niche across the United States. *Proc. Natl. Acad. Sci. U.S.A.* 114, 2946–2951 (2017).
- M. A. Cochrane, D. M. J. S. Bowman, Manage fire regimes, not fires. Nat. Geosci. 14, 455–457 (2021).

SCIENCE ADVANCES | RESEARCH ARTICLE

- M.-A. Parisien, Q. E. Barber, K. G. Hirsch, C. A. Stockdale, S. Erni, X. Wang, D. Arseneault, S. A. Parks, Fire deficit increases wildfire risk for many communities in the Canadian boreal forest. *Nat. Commun.* 11, 2121 (2020).
- S. Modugno, H. Balzter, B. Cole, P. Borrelli, Mapping regional patterns of large forest fires in Wildland-Urban interface areas in Europe. J. Environ. Manage. 172, 112–126 (2016).
- A. Bar Massada, V. C. Radeloff, S. I. Stewart, T. J. Hawbaker, Wildfire risk in the wildlandurban interface: A simulation study in northwestern Wisconsin. For. Ecol. Manage. 258, 1990–1999 (2009)
- J. P. Argañaraz, V. C. Radeloff, A. Bar-Massada, G. I. Gavier-Pizarro, C. M. Scavuzzo, L. M. Bellis, Assessing wildfire exposure in the Wildland-Urban Interface area of the mountains of central Argentina. *J. Environ. Manage.* 196, 499–510 (2017).
- S. Li, V. Dao, M. Kumar, P. Nguyen, T. Banerjee, Mapping the wildland-urban interface in California using remote sensing data. Sci. Rep. 12, 5789 (2022).
- V. Fernández-García, D. Beltrán-Marcos, L. Calvo, Building patterns and fuel features drive wildfire severity in wildland-urban interfaces in Southern Europe. *Landsc. Urban Plan.* 231, 104646 (2023).
- Y. Zhang, H. S. He, J. Yang, The wildland–urban interface dynamics in the southeastern U.S. from 1990 to 2000. *Landsc. Urban Plan.* 85, 155–162 (2008).
- M. L. Chas-Amil, J. Touza, E. García-Martínez, Forest fires in the wildland-urban interface: A spatial analysis of forest fragmentation and human impacts. *Appl. Geogr.* 43, 127–137 (2013)
- 32. M. Nielsen-Pincus, R. G. Ribe, B. R. Johnson, Spatially and socially segmenting private landowner motivations, properties, and management: A typology for the wildland urban interface. *Landsc. Urban Plan.* **137**, 1–12 (2015).
- M. Polinova, L. Wittenberg, H. Kutiel, A. Brook, Reconstructing pre-fire vegetation condition in the wildland urban interface (WUI) using artificial neural network. *J. Environ. Manage.* 238, 224–234 (2019).
- M. D. Caggiano, W.T. Tinkham, C. Hoffman, A. S. Cheng, T. J. Hawbaker, High resolution mapping of development in the wildland-urban interface using object based image extraction. *Heliyon* 2, e00174 (2016).
- F. J. Alcasena, C. R. Evers, C. Vega-Garcia, The wildland-urban interface raster dataset of Catalonia. Data Brief 17, 124–128 (2018).
- L. M. Johnston, M. D. Flannigan, Mapping Canadian wildland fire interface areas. Int. J. Wildland Fire 27, 1–14 (2017).
- B. Chen, S. Wu, Y. Jin, Y. Song, C. Wu, S. Venevsky, B. Xu, C. Webster, P. Gong, Wildfire risk for global wildland–urban interface areas. *Nat. Sustain.* 7, 474–484 (2024).
- A. E. Larsen, A. J. MacDonald, A. J. Plantinga, Lyme disease risk influences human settlement in the wildland-urban interface: Evidence from a longitudinal analysis of counties in the northeastern United States. Am. J. Trop. Med. Hyg. 91, 747–755 (2014).
- G. D. Jenerette, K. E. Anderson, M. L. Cadenasso, M. Fenn, J. Franklin, M. L. Goulden, L. Larios, S. Pincetl, H. M. Regan, S. J. Rey, L. S. Santiago, A. D. Syphard, An expanded framework for wildland–urban interfaces and their management. *Front. Ecol. Environ.* 20, 516–523 (2022)
- K. C. Seto, B. Güneralp, L. R. Hutyra, Global forecasts of urban expansion to 2030 and direct impacts on biodiversity and carbon pools. *Proc. Natl. Acad. Sci. U.S.A.* 109, 16083–16088 (2012).
- J. Chen, X. Cao, S. Peng, H. Ren, Analysis and applications of GlobeLand30: A review. ISPRS Int. J. Geo Inf. 6, 230 (2017).
- FAO, Guidelines on Fire Management in Temperate and Boreal Forests, (2002); www.fao. org/3/aq041e/aq041e.pdf.
- J. Chen, J. Chen, A. Liao, X. Cao, L. Chen, X. Chen, C. He, G. Han, S. Peng, M. Lu, W. Zhang, X. Tong, J. Mills, Global land cover mapping at 30m resolution: A POK-based operational approach. ISPRS J. Photogramm. Remote Sens. 103, 7–27 (2015).
- M. W. Jones, J. T. Abatzoglou, S. Veraverbeke, N. Andela, G. Lasslop, M. Forkel, A. J. P. Smith, C. Burton, R. A. Betts, G. R. van der Werf, S. Sitch, J. G. Canadell, C. Santín, C. Kolden, S. H. Doerr, C. Le Quéré, Global and regional trends and drivers of fire under climate change. Rev. Geophys. 60, e2020RG000726 (2022).
- S. S. Rabin, B. I. Magi, E. Shevliakova, S. W. Pacala, Quantifying regional, time-varying effects of cropland and pasture on vegetation fire. *Biogeosciences* 12, 6591–6604 (2015).
- L. Giglio, W. Schroeder, A global feasibility assessment of the bi-spectral fire temperature and area retrieval using MODIS data. *Remote Sens. Environ.* 152, 166–173 (2014).
- G. R. van der Werf, J. T. Randerson, L. Giglio, G. J. Collatz, M. Mu, P. S. Kasibhatla,
 D. C. Morton, R. S. DeFries, Y. Jin, T. T. van Leeuwen, Global fire emissions and the contribution of deforestation, savanna, forest, agricultural, and peat fires (1997–2009).
 Atmos. Chem. Phys. 10, 11707–11735 (2010).
- B. I. Magi, S. Rabin, E. Shevliakova, S. Pacala, Separating agricultural and non-agricultural fire seasonality at regional scales. *Biogeosciences* 9, 3003–3012 (2012).
- Y. Chen, D. C. Morton, N. Andela, G. R. van der Werf, L. Giglio, J. T. Randerson, A pan-tropical cascade of fire driven by El Niño/Southern Oscillation. *Nat. Clim. Change* 7, 906–911 (2017).
- Q. Zhong, N. Schutgens, G. R. van der Werf, T. van Noije, S. E. Bauer, K. Tsigaridis, T. Mielonen, R. Checa-Garcia, D. Neubauer, Z. Kipling, A. Kirkevåg, D. J. L. Olivié,

- H. Kokkola, H. Matsui, P. Ginoux, T. Takemura, P. Le Sager, S. Rémy, H. Bian, M. Chin, Using modelled relationships and satellite observations to attribute modelled aerosol biases over biomass burning regions. *Nat. Commun.* **13**, 5914 (2022).
- X. Liu, Y. Huang, X. Xu, X. Li, X. Li, P. Ciais, P. Lin, K. Gong, A. D. Ziegler, A. Chen, P. Gong, J. Chen, G. Hu, Y. Chen, S. Wang, Q. Wu, K. Huang, L. Estes, Z. Zeng, High-spatiotemporalresolution mapping of global urban change from 1985 to 2015. *Nat. Sustain.* 3, 564–570 (2020).
- S. Hantson, N. Andela, M. L. Goulden, J.T. Randerson, Human-ignited fires result in more extreme fire behavior and ecosystem impacts. *Nat. Commun.* 13, 2717 (2022).
- V. C. Radeloff, D. P. Helmers, M. H. Mockrin, A. R. Carlson, T. J. Hawbaker, S. Martinuzzi, The 1990–2020 wildland-urban interface of the conterminous United States - geospatial data (USDA Forest Service, ed. 3, 2022); https://doi.org/10.2737/rds-2015-0012-3.
- P. Potapov, M. C. Hansen, A. Pickens, A. Hernandez-Serna, A. Tyukavina, S. Turubanova, V. Zalles, X. Li, A. Khan, F. Stolle, N. Harris, X.-P. Song, A. Baggett, I. Kommareddy, A. Kommareddy, The global land cover and land use change dataset derived from the landsat archive: First results. Front. Remote Sens. 3, 856903 (2022).
- P. Gong, H. Liu, M. Zhang, C. Li, J. Wang, H. Huang, N. Clinton, L. Ji, W. Li, Y. Bai, B. Chen,
 B. Xu, Z. Zhu, C. Yuan, H. Ping Suen, J. Guo, N. Xu, W. Li, Y. Zhao, J. Yang, C. Yu, X. Wang,
 H. Fu, L. Yu, I. Dronova, F. Hui, X. Cheng, X. Shi, F. Xiao, Q. Liu, L. Song, Stable classification with limited sample: Transferring a 30-m resolution sample set collected in 2015 to mapping 10-m resolution global land cover in 2017. Sci. Bull. 64, 370–373 (2019).
- 56. P. Gong, J. Wang, L. Yu, Y. Zhao, Y. Zhao, L. Liang, Z. Niu, X. Huang, H. Fu, S. Liu, C. Li, X. Li, W. Fu, C. Liu, Y. Xu, X. Wang, Q. Cheng, L. Hu, W. Yao, H. Zhang, P. Zhu, Z. Zhao, H. Zhang, Y. Zheng, L. Ji, Y. Zhang, H. Chen, A. Yan, J. Guo, L. Yu, L. Wang, X. Liu, T. Shi, M. Zhu, Y. Chen, G. Yang, P. Tang, B. Xu, C. Gir, N. Clinton, Z. Zhu, J. Chen, J. Chen, Finer resolution observation and monitoring of global land cover: First mapping results with Landsat TM and ETM+ data. Int. J. Remote Sens. 34, 2607–2654 (2013).
- X. Zhang, L. Liu, X. Chen, Y. Gao, S. Xie, J. Mi, GLC_FCS30: Global land-cover product with fine classification system at 30 m using time-series Landsat imagery. *Earth Syst. Sci. Data* 13, 2753–2776 (2021).
- L. Giglio, W. Schroeder, C. O. Justice, The collection 6 MODIS active fire detection algorithm and fire products. *Remote Sens. Environ.* 178, 31–41 (2016).
- R. Ramo, E. Roteta, I. Bistinas, D. van Wees, A. Bastarrika, E. Chuvieco, G. R. van der Werf, African burned area and fire carbon emissions are strongly impacted by small fires undetected by coarse resolution satellite data. *Proc. Natl. Acad. Sci. U.S.A.* 118, 201116(118 (2021)
- N. Andela, D. C. Morton, L. Giglio, Y. Chen, G. R. van der Werf, P. S. Kasibhatla, R. S. DeFries, G. J. Collatz, S. Hantson, S. Kloster, D. Bachelet, M. Forrest, G. Lasslop, F. Li, S. Mangeon, J. R. Melton, C. Yue, J. T. Randerson, A human-driven decline in global burned area. Science 356, 1356–1362 (2017).
- A. Bento-Gonçalves, A. Vieira, Wildfires in the wildland-urban interface: Key concepts and evaluation methodologies. Sci. Total Environ. 707, 135592 (2020).
- 62. D. Caballero, I. Beltran, Concepts and ideas of assessing settlement fire vulnerability in the W-UI zone, in *Proceedings of the International Workshop WARM, in Forest Fires in the Wildland-Urban Interface and Rural Areas in Europe: An Integral Planning and Management Challenge*, G. Xanthopoulos, Ed. (2003), pp. 47–54.
- J. M. C. Pereira, Defining and mapping the wildland-urban interface in Portugal, in Advances in Forest Fire Research 2018, D. X. Viegas, Ed. (Imprensa da Universidade de Coimbra, 2018), pp. 742–749; http://dx.doi.org/10.14195/978-989-26-16-506_81.
- C. Lampin-Maillet, M. Jappiot, M. Long, C. Bouillon, D. Morge, J.-P. Ferrier, Mapping wildland-urban interfaces at large scales integrating housing density and vegetation aggregation for fire prevention in the South of France. *J. Environ. Manage.* 91, 732–741 (2010).
- D. Kahle, H. Wickham, ggmap: Spatial visualization with ggplot2. R J. 5, 144–161 (2013).
- 66. H. Hersbach, B. Bell, P. Berrisford, S. Hirahara, A. Horányi, J. Muñoz-Sabater, J. Nicolas, C. Peubey, R. Radu, D. Schepers, A. Simmons, C. Soci, S. Abdalla, X. Abellan, G. Balsamo, P. Bechtold, G. Biavati, J. Bidlot, M. Bonavita, G. De Chiara, P. Dahlgren, D. Dee, M. Diamantakis, R. Dragani, J. Flemming, R. Forbes, M. Fuentes, A. Geer, L. Haimberger, S. Healy, R. J. Hogan, E. Hólm, M. Janisková, S. Keeley, P. Laloyaux, P. Lopez, C. Lupu, G. Radnoti, P. de Rosnay, I. Rozum, F. Vamborg, S. Villaume, J.-N. Thépaut, The ERA5 global reanalysis. Quart. J. Roy. Meteor. Soc. 146, 1999–2049 (2020).
- CMES, Fire danger indices historical data from the Copernicus Emergency Management Service, ECMWF (2019); https://doi.org/10.24381/CDS.0E89C522.
- C. Vitolo, F. Di Giuseppe, C. Barnard, R. Coughlan, J. San-Miguel-Ayanz, G. Libertá,
 Krzeminski, ERA5-based global meteorological wildfire danger maps. Sci. Data 7, 216 (2020)
- K. Winkler, R. Fuchs, M. Rounsevell, M. Herold, Global land use changes are four times greater than previously estimated. *Nat. Commun.* 12, 2501 (2021).
- WorldPop, Center for International Earth Science Information Network (CIESIN), Columbia University, Global high resolution population denominators project (2018); https://doi. org/10.5258/SOTON/WP00647.

SCIENCE ADVANCES | RESEARCH ARTICLE

- G. R. van der Werf, J. T. Randerson, L. Giglio, T. T. van Leeuwen, Y. Chen, B. M. Rogers, M. Mu, M. J. E. van Marle, D. C. Morton, G. J. Collatz, R. J. Yokelson, P. S. Kasibhatla, Global fire emissions estimates during 1997–2016. *Earth Syst. Sci. Data* 9, 697–720 (2017).
- J.T. Abatzoglou, A. P. Williams, Impact of anthropogenic climate change on wildfire across western US forests. Proc. Natl. Acad. Sci. U.S.A. 113, 11770–11775 (2016).
- 73. K. Shi, Y. Touge, Characterization of global wildfire burned area spatiotemporal patterns and underlying climatic causes. *Sci. Rep.* **12**, 644 (2022).
- T.V. Nguyen, K. J. Allen, N. C. Le, C. Q. Truong, K. Tenzin, P. J. Baker, Human-driven fire regime change in the seasonal tropical forests of central Vietnam. *Geophys. Res. Lett.* 50, e2022GL100687 (2023).
- V. Iglesias, J. K. Balch, W. R. Travis, U.S. fires became larger, more frequent, and more widespread in the 2000s. Sci. Adv. 8, eabc0020 (2022).
- W. J. de Groot, B. M. Wotton, M. D. Flannigan, Wildland fire danger rating and early warning systems, in Wildfire Hazards, Risks and Disasters, J. F. Shroder, D. Paton, Eds. (Elsevier, 2015), chap. 11, pp. 207–228; www.sciencedirect.com/science/article/pii/ B9780124104341000117.
- Forest Service, Bureau of Indian Affairs, Bureau of Land Management, Fish and Wildlife Service & National Park Service, Urban wildland interface communities within the vicinity of federal lands that are at high risk from wildfire. (Forest Service, USDA, 2001).

Acknowledgments

Funding: This work was supported by Strategic Priority Research Program of the Chinese Academy of Sciences (XDB0740100), the National Natural Science Foundation of China (42222110), and the National Key Research and Development Program of China (no. 2022YFF1301101). The funders had no role in the conceptualization, design, data collection, analysis, decision to publish, or preparation of the manuscript. **Author contributions:**

Conceptualization: J.W., Y.Gu., Y. Ge and C.Z. Methodology: Y.Gu., J.W., and C.Z. Data and analysis: Y.Gu., J.W., Y. Ge., and C.Z. Visualization: Y.Gu., J.W., Y. Ge, and C.Z. Supervision: Y.Gu., J.W., Y. Ge, and C.Z. Writing—original draft: Y.Gu., J.W., Y. Ge, and C.Z. Writing—review and editing: Y.Gu., J.W., Y. Ge, and C.Z. Funding acquisition: J.W. Competing interests: The authors declare that they have no competing interests. Data and materials availability: All data needed to evaluate the conclusions in the paper are present in the paper and the Supplementary Materials. The GlobeLand30 land cover datasets are publicly available at www. webmap.cn/. The MODIS active fire datasets are available at https://firms.modaps.eosdis.nasa. gov/download/. The HILDA+ vGLOB-1.0 land cover datasets are available at https://doi. org/10.1594/PANGAEA.921846. The Fire Weather Index historical data are available at https:// ewds.climate.copernicus.eu/datasets/cems-fire-historical-v1?tab=overview. The daily maximum temperature data are available at https://cds.climate.copernicus.eu/datasets/ derived-era5-pressure-levels-daily-statistics?tab=overview. The WorldPop population datasets are publicly through WorldPop Open Population Repository at the following link: https://wopr. worldpop.org/. The GFED regions are derived from GFED ancillary data, available at www.geo. vu.nl/~gwerf/GFED/GFED4/. The WUI maps produced by United State Forest Service are available at www.fs.usda.gov/rds/archive/catalog/RDS-2015-0012-3. The WUI map produced by California Fire and Resource Assessment Program is available at frap.fire.ca.gov. The 30-m WUI mapping results in 2000, 2010, and 2020 produced by this study are available in a public data repository at https://zenodo.org/records/13745109. The code to draw figures is shared at https://github.com/CASGIS/GlobalWUI.

Submitted 28 February 2024 Accepted 7 October 2024 Published 8 November 2024 10.1126/sciadv.ado9587